Photoconductive generation and detection of THz-bandwidth pulses using near-field coupling to a free-space metallic slit waveguide

Robert Smith, Afshin Jooshesh, Jinye Zhang, and Thomas Darcie

October 2017

Research Article | Vol. 25, No. 22 | 30 Oct 2017 | OPTICS EXPRESS 26492
Optics EXPRESS

Photoconductive generation and detection of THz-bandwidth pulses using near-field coupling to a free-space metallic slit waveguide

ROBERT SMITH,* AFSHIN JOOSHESH, JINYE ZHANG, AND THOMAS DARCIE

Department of Electrical and Computer Engineering, University of Victoria, Victoria, BC V8P 5C2, Canada
*levismit@uvic.ca

Abstract: THz-bandwidth pulses are generated, transmitted along a gold-plated stainless steel metallic slit waveguide, and detected with a 1.5 THz bandwidth and 60 dB dynamic range. The source and detector were edge-pumped slotlines on LT-GaAs placed within the near-field region of the waveguide entrance and exit aperture. The motivation for this work was to develop a complete dispersion-free THz system which was simple to manufacture and could be utilized for free-space waveguide experimentation.

OCIS codes: (300.6495) Spectroscopy, terahertz; (250.3140) Integrated optoelectronic circuits; (250.5530) Pulse propagation and temporal solitons; (250.6715) Switching.

References and links

1. D. Auston, "Impulse response of photoconductors in transmission lines," IEEE J. Quantum Electron. **19**, 639–648 (1983).
2. D. Auston, *Picosecond Photoconductors: Physical Properties and Applications* (Academic Press, 1984).
3. M. B. Ketchen, D. Grischkowsky, T. C. Chen, C.-C. Chi, I. N. Duling, N. J. Halas, J.-M. Halbout, J. A. Kash, and G. P. Li, "Generation of subpicosecond electrical pulses on coplanar transmission lines," Appl. Phys. Lett. **48**, 751–753 (1986).
4. D. Grischkowsky, M. Ketchen, C.-C. Chi, I. Duling, N. Halas, J.-M. Halbout, and P. May, "Capacitance free generation and detection of subpicosecond electrical pulses on coplanar transmission lines," IEEE J. Quantum Electron. **24**, 221–225 (1988).
5. D. Krökel, D. Grischkowsky, and M. B. Ketchen, "Subpicosecond electrical pulse generation using photoconductive switches with long carrier lifetimes," Appl. Phys. Lett. **54**, 1046–1047 (1989).
6. D. Rutledge, D. Neikirk, and D. Kasilingam, *Integrated-Circuit Antennas* (Academic Press, 1983).
7. J. Nees, S. Williamson, and G. Mourou, "100 GHz traveling-wave electro-optic phase modulator," Appl. Phys. Lett. **54**, 1962–1964 (1989).
8. H. Cheng, J. Whitaker, T. Weller, and L. Katehi, "Terahertz-bandwidth pulse propagation on a coplanar stripline fabricated on a thin membrane," IEEE Microw. Guided Wave Lett. **4**, 89–91 (1994).
9. M. Wächter, M. Nagel, and H. Kurz, "Metallic slit waveguide for dispersion-free low-loss terahertz signal transmission," Appl. Phys. Lett. **90**, 061111 (2007).
10. M. Wächter, M. Nagel, and H. Kurz, "Low-loss terahertz transmission through curved metallic slit waveguides fabricated by spark erosion," Appl. Phys. Lett. **92**, 161102 (2008).
11. R. Smith, F. Ahmed, A. Jooshesh, J. Zhang, M. Jun, and T. Darcie, "THz field enhancement by antenna coupling to a tapered thick slot waveguide," J. Lightwave Technol. **32**, 15878 (2014).
12. R. Smith, A. Jooshesh, J. Zhang, and T. Darcie, "THz-TDS using a photoconductive free-space linear tapered slot antenna transmitter," Opt. Express **25**, 10118 (2017).
13. H. Zhan, R. Mendis, and D. M. Mittleman, "Superfocusing terahertz waves below λ/250 using plasmonic parallel-plate waveguides," Opt. Express **18**, 9643 (2010).
14. M. Wächter, M. Nagel, and H. Kurz, "Tapered photoconductive terahertz field probe tip with subwavelength spatial resolution," Appl. Phys. Lett. **95**, 041112 (2009).
15. S. Sawallich, B. Globisch, C. Matheisen, M. Nagel, R. Dietz, and T. Göbel, "Photoconductive terahertz near-field detectors for operation with 1550-nm pulsed fiber lasers," IEEE Trans. Terahertz Sci. Technol. **6**, 365–370 (2016).
16. M. Nagel, A. Michalski, and H. Kurz, "Contact-free fault location and imaging with on-chip terahertz time-domain reflectometry," Opt. Express **19**, 12509–12514 (2011).
17. G. Veronis and S. Fan, "Modes of subwavelength plasmonic slot waveguides," J. Lightwave Technol. **25**, 2511–2521 (2007).
18. J. Xiao, Q.-Q. Wei, D.-G. Yang, P. Zhang, N. He, G.-Q. Zhang, and X.-P. Chen, "Hybrid plasmonics slot THz waveguide for subwavelength field confinement and crosstalk between two waveguides," IEEE J. Sel. Top. Quantum

#304582 https://doi.org/10.1364/OE.25.026492
Journal © 2017 Received 10 Aug 2017; revised 4 Oct 2017; accepted 5 Oct 2017; published 16 Oct 2017

Optics EXPRESS

Electron. **23**, 1–5 (2017).
19. S. Gupta, M. Y. Frankel, J. A. Valdmanis, J. F. Whitaker, G. A. Mourou, F. W. Smith, and A. R. Calawa, "Subpicosecond carrier lifetime in GaAs grown by molecular beam epitaxy at low temperatures," Appl. Phys. Lett. **59**, 3276–3278 (1991).
20. Y.-H. Lee, *Principles of Terahertz Science and Technology* (Springer, 2009).
21. L. Duvillaret, F. Garet, J.-F. Roux, and J.-L. Coutaz, "Analytical modeling and optimization of terahertz time-domain spectroscopy experiments, using photoswitches as antennas," IEEE J. Sel. Top. Quantum Electron. **7**, 615–623 (2001).

1. Introduction

Photoconductive pulse generation and detection on a substrate was investigated in the 1980s [1–5]. In [1] the theory of photoconductive pulse generation and detection was investigated. This theory was expanded upon in [2] where experimental results were provided. In [3] THz-bandwidth pulses are generated and transmitted along an 8mm coplanar transmission line and the "sliding contact" excitation method was introduced. The results of [3] are re-analyzed in [4] and conclude that a sliding contact source or detector can have no capacitance. In [5] the sliding contact is slightly modified to generate short pulses from a long-carrier-lifetime substrate. This was achieved by asymmetrically exciting the transmission line.

In the previously cited work the transmission lines consisted of metallic contacts deposited on a thick dielectric substrate. This configuration is undesirable because of leaky-wave radiation [6]. Leaky-wave radiation can be minimized by reducing the waveguide width or homogenizing the dielectric. To approximate a homogeneous dielectric a superstrate with same dielectric constant as the substrate can be placed [7], or the substrate can be thinned (<2 μm) to approximate the loss and dispersion of an air dielectric [8].

In this paper we use a metallic slit waveguide (MSWG) for low-loss and dispersion-free waveguiding [9–13]. In [9–11] a relatively thick (>300 μm) MSWG was excited by coupling the radiated field generated by a photoconductive switch. In [12] near-field excitation of a relatively thin (127 μm) copper MSWG was performed and used as a linear tapered slot antenna. In other works [14–16] near-field detectors have been utilized for surface conductivity and transverse field mapping. Plasmonic MSWGs have also been investigated in the optical [17] and THz regimes [18].

The novelty of this paper arises from the designed THz system. The system provides an effective and simplistic method for generating, transmitting, and detecting dispersion-free THz-bandwidth pulses which is not found elsewhere. The method of waveguide excitation is similar to past work [12], but here the THz source is a DC biased edge-pumped slotline which minimizes the pulse distortion by eliminating reflections associated with the bias lines. THz field transmission along a free-space MSWG is found elsewhere [9–12], but in this work a thinner gold-plated steel MSWG is utilized for broadband transmission. Also the MSWG includes tapers to reduce attenuation which is unique to this work. THz field detection is achieved by tapering the MSWG onto an edge-pumped slotline detector which located within the near-field region of the exit aperture of MSWG. We were unable to find a similar detector in other work. Other near-field detectors exist [14–16] which could potentially be utilized, but the manufacturing procedure for these detectors is difficult in comparison to a simple cleaved slotline.

2. Design

We have designed a THz system [Fig. 1] which uses a MSWG to overcome the issue of leaky-wave radiation, loss, and dispersion associated with substrate-based waveguides. The MSWG and slotline are excited by an optical pulse illuminating the biased slotline [Fig. 1(b)]. The generated field is transmitted along the MSWG and detected at the receiver [Fig. 1(c)]. Cross-sections of the MSWG and slotline are shown in Figs. 1(e)-1(f). Figure 1(d) illustrates the configuration of the experimental structure.

Optics EXPRESS

The thickness, T, of the MSWG should be selected based on the system bandwidth and excitation configuration. In [12] we identified detrimental Fabry-Pérot oscillations which are excited when a thick MSWG is asymmetrically excited by a current line (similar to the source presented here). These oscillations are present when the MSWG thickness, T, is comparable to the spatial pulse length in the metallic-slit waveguide (which is approximately equal to the spatial pulse length in air because the effective relative permittivity of the MSWG is ≈1). For example, if a MSWG is excited with a 0.5 ps pulse then T $\ll 150\mu$m.

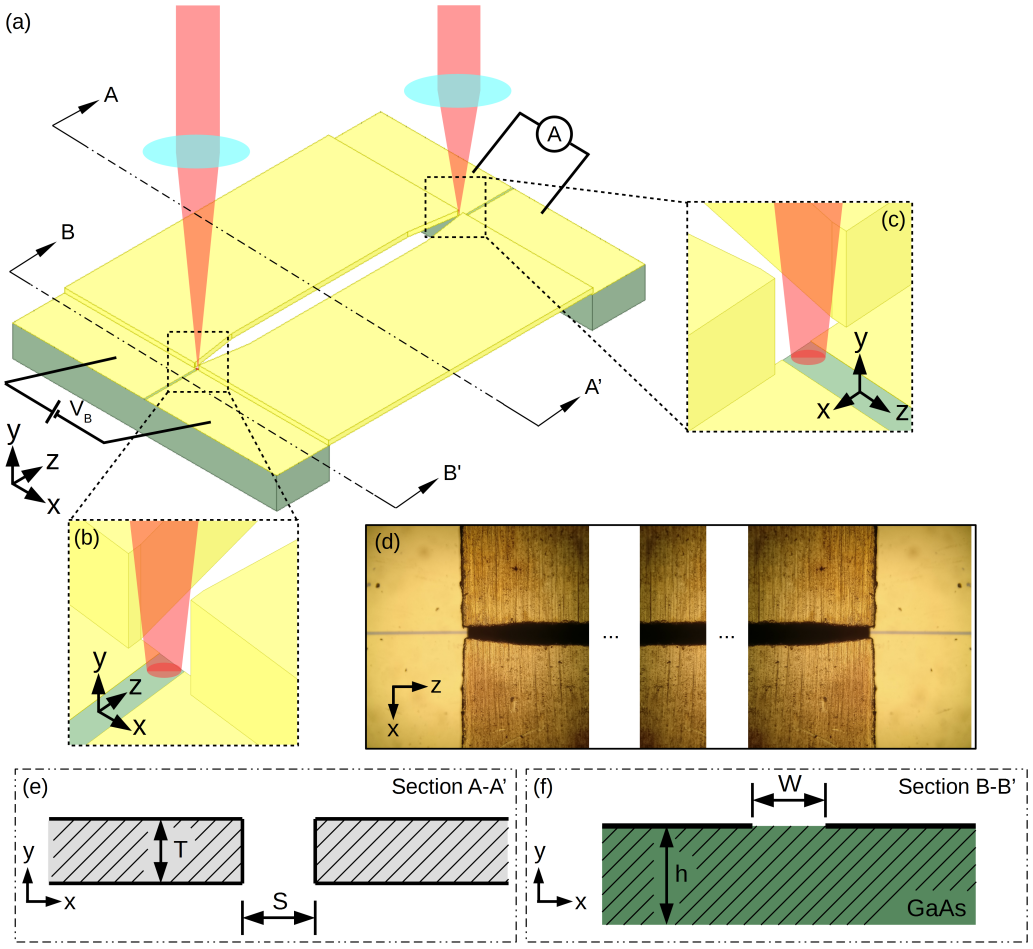

Fig. 1. Design of the THz system. (a) Overall structure. (b) Transmitter active area and optical excitation location. (c) Receiver active area and optical excitation location. (d) Configuration of experimental structure (top-down view). (e) Cross-section of MSWG and definitions. (f) Cross-section of slotline and definitions.

Figure 2 illustrates the circuit diagram which approximates the THz system. A DC bias voltage (90 V) is applied to the transmitter active area using a slotline. The transmitter active area is illuminated by a femtosecond optical pulse resulting in a conductance spike in $g_1(t)$. The current spike through $g_1(t)$ drives both the slotline and MSWG. Ideally no power should be delivered to the slotline but this is difficult to incorporate without introducing unwanted resonances due to discontinuous bias lines. A portion of the signal is near-field coupled across an air-gap (DC block) from the slotline into the MSWG which travels along a tapered section of waveguide to

Optics EXPRESS

reach a geometry with a lower attenuation coefficient. To maximize the signal coupled into the MSWG from the slotline the air-gap should be small (discussed later in Section 3). To minimize the radiation into free-space (and maximize coupling into the MSWG) the separation, S, at the start of the taper should be close to the slotline gap width (W = 20 μm) or slightly larger (such that the active area is not blocked from the optical pump). The MSWG was positioned by-hand and we were able to achieve S = 80 μm at the start of the taper which proved to be sufficient since we detected a signal. For the work presented here we pre-selected to machine a slight 40 μm taper into the MSWG plates so the transmitted field would remain confined to an area close to the free-space spatial pulse length. Given that we were able to position the start of the MSWG with a separation of S = 80 μm, this corresponded to separation of S = 160 μm at the end of the taper which resulted in an appreciable reduction in the attenuation coefficient [Fig. 3]. After the taper the pulse travels the length of the MSWG for 24 mm before tapering to the receiver. A portion of the signal couples to the receiver which generates a detectable DC current proportional to the product of the incident signal voltage and receiver conductance. The cross-correlation trace is produced by sweeping the relative time delay between the two signals via an optical delay line.

The MSWG material and thickness was selected to have acceptable mechanical strength and Fabry-Pérot oscillation reduction. As the waveguide becomes thinner the bend strength degrades but the adverse effects of Fabry-Pérot oscillations are minimized. In the limit of T $\rightarrow$ 0 μm, the metallic slit becomes a free-space slotline and the oscillations are eliminated, but this is impossible to achieve (or approximate) while maintaining mechanical strength. Copper with a thickness less than 100 μm is delicate therefore steel was used. The MSWG was fabricated using 0.002" (T = 51 μm) 304 stainless steel via wire electrical discharge machining (EDM) then gold-plated (plating thickness $\approx$ 1.5 μm).

The THz source and detector are identical W = 20 μm slotlines made of Ti/Au (5 nm/100 nm) RF sputtered on a 1 μm low-temperature Gallium Arsenide (LT-GaAs) epilayer. LT-GaAs is a sub-picosecond carrier-lifetime photoconductive material [19] which is commonly used for detecting THz pulses [20]. The LT-GaAs epilayer was grown on a semi-insulating Gallium Arsenide (SI-GaAs) substrate (h = 350 μm) which was annealed for 60 seconds at 600°C. Slotlines were selected because they do not introduce unwanted cavity resonances and are simple to manufacture (lithography, deposition, lift-off, then cleave at any point). Compared to our previous source [12], we expect that the transmitter losses a portion of the power to the slotline but the signal transmitted into the MSWG will have less distortion.

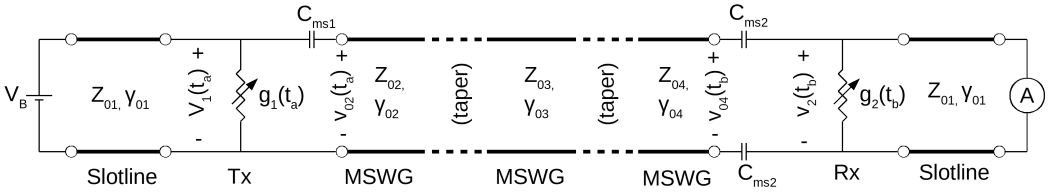

Fig. 2. Transmission line representation of circuit

3. Simulation

The structure was simulated in both time and frequency domain using Ansys HFSS v18. For all time-domain simulations the substrates are lossless GaAs with the relative permittivity set to $\epsilon_r = 12.9$ and the conductors set to perfect electric conductors (PECs). For the frequency-domain simulation the substrates are lossless GaAs with the relative permittivity set to $\epsilon_r = 12.9$ and the MSWG conductors are set to gold with conductivity of $\sigma_{Au} = 4.1 \times 10^7 S/m$. The frequency-domain simulation was used to calculate waveguide parameters $\alpha(f, S)$ and $Z_0(f, S)$

Optics EXPRESS

[Fig. 3]. The attenuation coefficient is dominated by conductor loss which was determined by comparing simulations with MSWG set to a PEC and gold. The attenuation coefficient at the entrance and exit of the MSWG is α(2 THz, 80 μm) = 0.099 dB/mm. The central section has an attenuation coefficient of α(2 THz, 160 μm) = 0.054 dB/mm. The difference between these attenuation coefficients is the reason for the taper. By doubling S the attenuation coefficient is approximately halved (note this does not scale linearly).

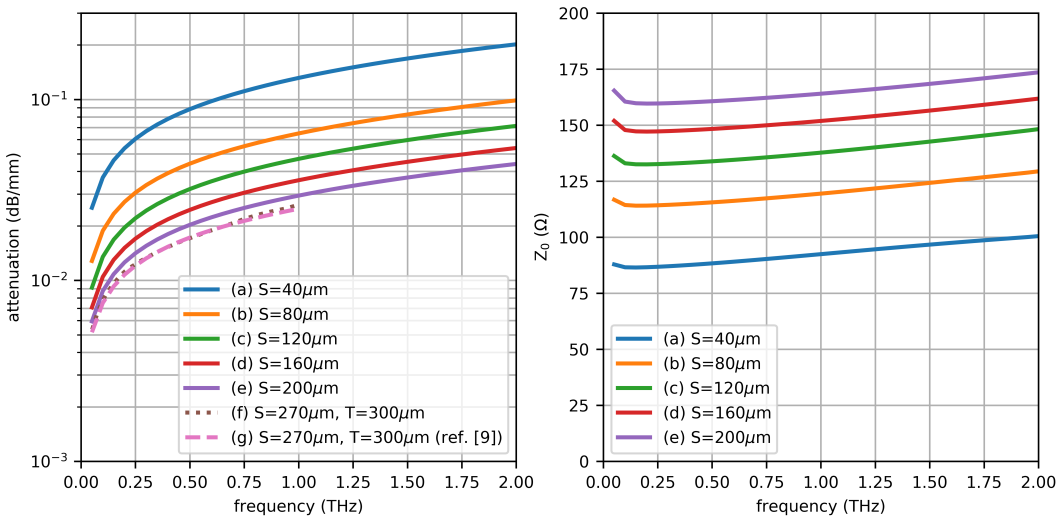

Fig. 3. MSWG attenuation solved with Ansys HFSS. The attenuation for various separations is plotted. Traces (f)-(g) are plotted to verify that our simulation results align with the results presented in [9]. The real part of the Z_{0pv} characteristic impedance is also plotted.

Time-domain simulations were used to visualize pulse coupling and transmission in a similar method to experimentation [Fig. 4]. For all transient simulations the source was a current source with the pulse shape defined by the normalized form of Eqn. 1 where the parameters where obtained from the experimental fit (τ_p = 0.21 ps, τ_c = 0.39 ps, τ_s = 0.08 ps). For the transient simulations the length of the central section of MSWG was reduced from 24 mm to 3 mm to reduce the simulation time. Videos for the transient simulations are included in the **Supplementary Material** to better illustrate the pulse propagation. The voltage at the receiver was calculated by integrating the E-field, $v_2(t) = \int \vec{E}(t) \cdot d\vec{l}$ at each time step. In Section 5 the simulated receiver voltage is used to fit the experimental data.

Optics EXPRESS

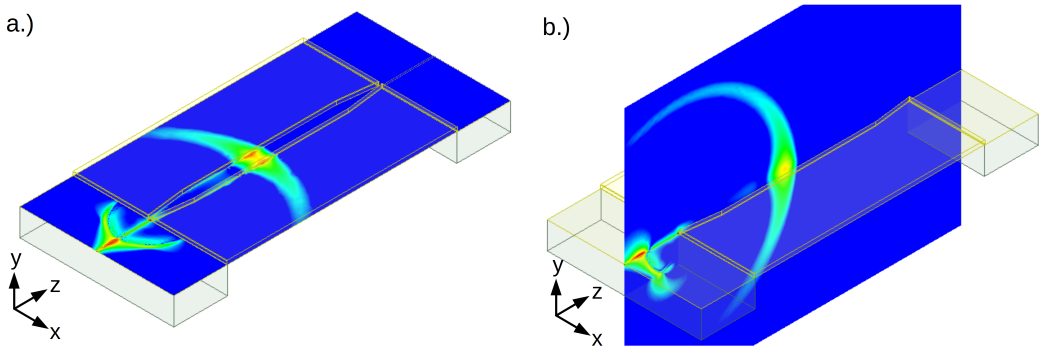

Fig. 4. Time-domain simulation illustrating the field coupled into MSWG 4 ps after excitation. The MSWG was set to a PEC. W=20μm, S=80μm→160μm. a) xz-plane (for video see Visualization 1). b) yz-plane (for video see Visualization 2).

The slotline to MSWG transition was investigated using a time-domain simulation with ideal material parameters (PECs and lossless dielectrics). The simulated structure consisted of a slotline coupled to a MSWG (without a taper or receiver). Figure 5 plots the results of the simulation which illustrates that the pulse is not heavily distorted by the introduction of a gap and that the relative attenuation remains less than 6dB for the gap size investigated in this paper.

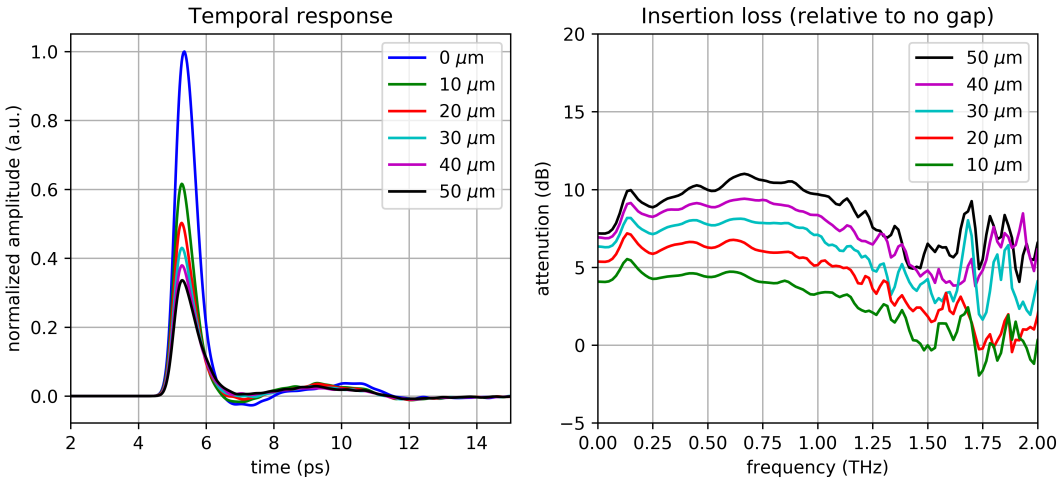

Fig. 5. Time-domain simulation which illustrates the field coupled to the MSWG from the slotline for a selection of gap sizes between the slotline and MSWG. S = 80 μm, W = 20 μm, T = 51 μm. a) Temporal response for various gap sizes normalized to the case without a gap. b) Frequency-dependent attenuation for various gap sizes relative to the case without a gap.

4. Experiment

A 780nm mode-locked femtosecond laser generated 80 fs pulses with an 80 MHz repetition for the experiment [Fig. 6]. The average optical power delivered to the transmitter and receiver was ≈15 mW. A photoconductive slotline transmitter and receiver were placed at the entrance and exit of a MSWG [Figs. 1(b)-1(c)]. The slotline and MSWG overlapped by approximately 20 μm. At the transmitter the slotline physically contacted one plate of the MSWG. At the receiver the slotline does not contact the MSWG and was separated by a small gap (≈10 μm). This configuration was

Optics EXPRESS

selected to minimize the low-frequency modulation of the optical chopper from being detected (which would appear as a DC offset).

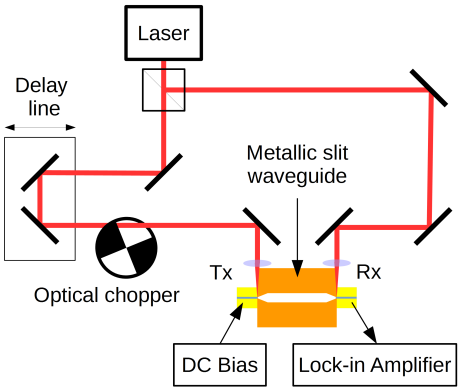

Fig. 6. Experimental setup. An 80 fs 780 nm laser beam is split into two paths, one directed to the transmitter through a mechanical delay line for THz generation, the other directed to the receiver for detection. A 25 mm MSWG connects the slotline based transmitter and receiver.

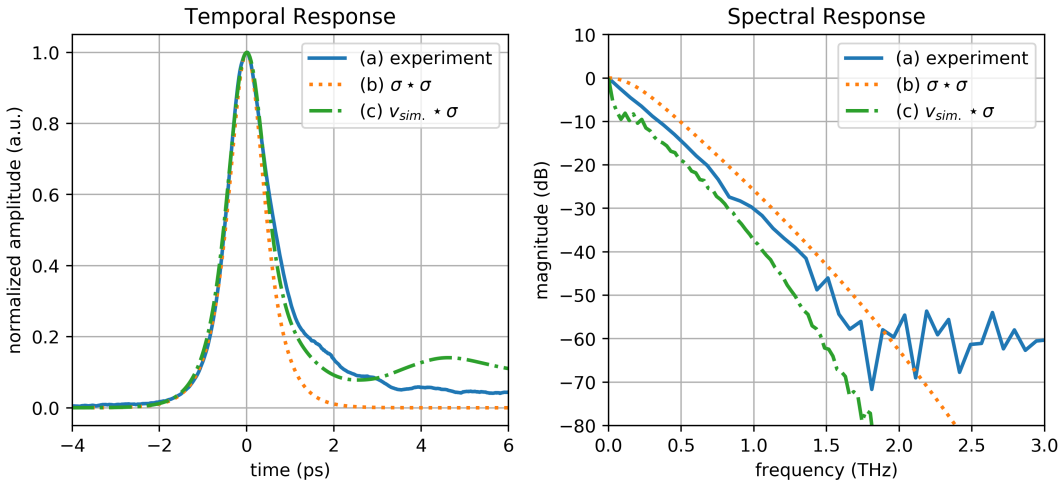

Fig. 7. Time-domain signals and respective Discrete Fourier Transform (DFT). (a) Experimental signal detected using the designed structure. (b) Autocorrelation of Eq. (1) fitted to signal (τ_p = 0.21 ps, τ_c = 0.39 ps, τ_s = 0.08 ps). (c) Simulated response, the receiver voltage was obtained with Ansys HFSS transient, the conductivity was obtained from Eq. (1).

5. Discussion

Figure 7 plots the measured results for the experiment illustrated in Fig. 6. The detected pulse proves that we are able generate, transmit (25 mm), and receive a THz-bandwidth pulse using a thin gold-coated steel MSWG. Use of near-field coupling of slotlines to the transmitter and receiver allows for a simple alignment with a non-resonant broadband response which is a desirable attribute for undistorted pulse transmission.

Optics EXPRESS

In this paper we are primarily concerned with the temporal profile of the received pulse. Many factors affect the amplitude therefore constant scaling factors are negated for curve fitting. The voltage across the transmitter active area is represented by $v_1(t)$, the conductance of the source active area is given by $g_1(t)$, and the substrate conductivity of the transmitter and receiver is given by $\sigma_1(t)$ and $\sigma_2(t)$, respectively. Given that $v_1(t) \propto g_1(t) \propto \sigma_1(t)$ [4, 20, 21] the curves will be fit based on normalized Eqn. (1) [20]:

$$\sigma_1(t) = \sigma_2(t) \propto \exp\left(\frac{\tau_p^2}{4\tau_c^2} - \frac{t}{\tau_c}\right) \cdot \operatorname{erfc}\left(\frac{\tau_p}{2\tau_c} - \frac{t}{\tau_p}\right) - \exp\left(\frac{\tau_p^2}{4\tau_{cs}^2} - \frac{t}{\tau_{cs}}\right) \cdot \operatorname{erfc}\left(\frac{\tau_p}{2\tau_{cs}} - \frac{t}{\tau_p}\right), \quad (1)$$

where τ_p is the square-root of the sum of squares of laser pulse width and carrier transit time [4], τ_c is the substrate carrier lifetime, τ_s is the substrate momentum relaxation time, $\tau_{cs} = (\tau_c^{-1} + \tau_s^{-1})^{-1}$, and erfc(x)=1-erf(x)=$2/\sqrt{\pi}\int_x^\infty e^{-t^2} dt$.

Experimentally the average current measured at the receiver is given by the time integral of the cross-correlation [3] of the induced voltage across the receivers active area, $v_2(t)$, and the sampling substrate conductance, $g_2(t)(\propto \sigma_2(t))$. To generate the plot shown in Fig. 7(a) the relative delay between the two signals ($v_2(t)$ and $g_2(t)$) is swept via an optical delay line.

Observation of Fig. 7 reveals that the detected pulse is a baseband signal which contains a DC component in the Discrete Fourier Transform (DFT). This may cause confusion because there are gaps between the slotlines and MSWG which should block the DC component. This can be explained by a couple points. First, the detected current, at a given delay, is obtained by the convolution of $v_2(t)$ and $g_2(t)$ which implies the average detected current does not directly correspond to $v_2(t)$. Next, given the relatively narrow temporal window (10 ps) the DC component appears large, if the temporal window length was substantially larger, the DC component would be heavily reduced. Finally, the detected signal was scaled between zero and one which modified the DC component.

Figure 7(b) was fitted to the experimental results by starting with common initial time constants (τ_p^0 = 0.18 ps, τ_c^0 = 0.5 ps, τ_s^0 = 0.03 ps) then adjusting until they fit the experimental results, which occurs when τ_p = 0.21 ps, τ_c = 0.39 ps, τ_s = 0.08 ps. Of these values the only parameter which can be easily modified is the carrier transit time (contained in τ_p) which could potentially increase the bandwidth. We selected to use a W = 20 μm slotline primarily because we had that lithography mask available. It is presumed that by reducing W, the reduced carrier transit time will result in a wider bandwidth.

Figure 7(c) is the result of a transient simulation which is numerically cross-correlated with the normalized conductivity function, Eq. (1). Figure 7(c) illustrates that the leading edge of the detected pulse is relatively undistorted by traversing the MSWG.

6. Conclusion

We have demonstrated THz-bandwidth pulse generation, transmission and detection over a MSWG, showing that using near-field coupling for waveguide excitation and detection can be both simple and effective. Dispersion-free transmission is achieved over 25 mm with a bandwidth of 1.5 THz. Comparison with a theoretical model suggests bandwidth is limited by carrier transit time which will be reduced in subsequent photoconductor designs.

Funding

Natural Science and Engineering Research Council (NSERC) Canada.